Journal Name

Crossmark

RECEIVED
dd Month yyyy

REVISED
dd Month yyyy

PAPER

XFEL Imaging Techniques for High Energy Density and Inertial Fusion Energy Research at HED-HiBEF

Alejandro Laso Garcia[1,*], Mikhail Mishchenko[2], Victorien Bouffetier[1], Gabriel Pérez-Callejo[3], Karen Appel[2], Alexey Arefiev[4], Carsten Baehtz[1], Erik Brambrink[2], Mihail O. Cernaianu[5], Domenico Doria[5], Tobias Dornheim[1,14], Gillis M. Dyer[6], Nicolas Fefeu[7], Eric Galtier[6], Thomas Gawne[14,1], Petru Ghenuche[5], Sebastian Goede[2], Johannes Hagemann[8], Marie-Luise Herbert[1,9], Hauke Höppner[1], Lingen Huang[1], Oliver S. Humphries[2], Mae Jones[12], Dimitri Khaghani[6], Thomas Kluge[1], Jayanath Koliyadu[2], Dominik Kraus[1], Hae Ja Lee[6], Julian Lütgert[9], Mikako Makita[2], Jean-Paul Naedler[9], Bob Nagler[6], Motoaki Nakatsutsumi[2], Quynh L. Nguyen[6], Alexander Pelka[1], Thomas R. Preston[2], Chong Bing Qu[9], Sripati V. Rahul[2], Lisa Randolph[10], Ronald Redmer[9], Martin Rehwald[1], Hans G. Rinderknecht[11], Angel Rodriguez-Fernandez[2], Joao J. Santos[7], Ulrich Schramm[1], Michal Smid[1], Cornelius Strohm[8], Jergus Strucka[2,13], Minxue Tang[2], Patrik Vagovic[2,8], Milenko Vescovi[1], Long Yang[1], Karl Zeil[1], Ulf Zastrau[2], Thomas E. Cowan[1], Toma Toncian[1]

[1]Helmholtz-Zentrum Dresden - Rossendorf, Dresden, 01328 Germany
[2]European XFEL, Schenefeld, 22869 Germany
[3]Departamento de Física Teórica, Atómica y Óptica, Universidad de Valladolid, Valladolid, 47011 Spain
[4]Department of Mechanical and Aerospace Engineering, University of California San Diego, La Jolla, California 92093, USA
[5]Extreme Light Infrastructure - Nuclear Physics, IFIN-HH, 077125 Măgurele, Romania
[6]SLAC National Accelerator Laboratory, Menlo Park, 94025 USA
[7]CNRS - Université de Bordeaux, CELIA, Talence, F-33405 France
[8]DESY Deutsches Elektronen-Synchrotron, Photon Science, Hamburg, 22607 Germany
[9]Universität Rostock, Institut für Physik, Rostock, D-18059 Germany
[10]Universität Siegen, Department Physik, Siegen, 57072 Germany
[11]Laboratory for Laser Energetics, University of Rochester, Rochester, New York 14623, USA
[12]The University of Edinburgh, School of Physics and Astronomy, Edinburgh, EH9 3FD United Kingdom
[13]Plasma Physics Group, Imperial College London, London, SW7 2AZ United Kingdom
[14]Center for Advanced Systems Understanding (CASUS), Görlitz, D-02826 Germany
[*]Author to whom any correspondence should be addressed.

E-mail: a.garcia@hzdr.de

Keywords: x-ray imaging, XFEL, high energy density, inertial fusion energy

Abstract

The imaging platform developed at the High Energy Density - Helmholtz International Beamline for Extreme Fields (HED-HiBEF) instrument at the European XFEL and its applications to high energy density and fusion related research are presented. The platform combines the XFEL beam with the high-intensity short-pulse laser ReLaX and the high-energy nanosecond-pulse laser DiPOLE-100X. The spatial resolution is better than 500 nm and the temporal resolution of the order of 50 fs. The influence of the XFEL source in the x-ray imaging method is discussed. Free-propagation x-ray phase contrast imaging and Talbot-Lau imaging setups are shown. We show examples of blast waves and converging cylindrical shocks in aluminium, resonant absorption measurements of specific charged states in copper with ReLaX and planar shocks in polystyrene material generated by DiPOLE-100X. For the first time, we show the application of Talbot-Lau interferometry to convergent cylindrical shocks as well as resonant absorption processes. We also discuss the possibilities introduced by combining this imaging platform with a kJ-class laser.

1 Introduction

Probing high energy density states of matter is a challenging task. The short time scales (from fs to tens of ns), the small spatial scales (of nanometer to tens of micrometers) and the high electron densities require the use of short, bright x-ray beams. Several variations of x-ray imaging have been

developed depending on the sample parameters (size, optical thickness, index of refraction for the used x-ray energy): absorption radiography is used for optically thick targets where absorption is dominant, phase-contrast imaging for optically thin samples where absorption is negligible, grating interferometry and Talbot-Lau grating interferometry to further increase sensitivity and accuracy by exploiting the Talbot effect.

In optical laser facilities, x-ray imaging has been mostly implemented via laser-based x-ray backlighters [1, 2, 3, 4, 5], providing novel insight on the dynamic of shock generation and propagation in planar geometries at LULI [6, 7]), in direct drive configuration at OMEGA [8] and at the National Ignition Facility, imaging of capsule implosions has even provided crucial information on the influence of the tent holder [9]. Two-grating interferometry has also been developed, with a phase grating and an analyzer grating [10]. However, all these techniques have limited temporal resolution, down to the picosecond range, due to the duration of the laser generated x-ray pulse, or the gating duration on x-ray framing cameras [11]. They also suffer from limitations on the spatial resolution, typically in the range of micrometers. Imaging with the betatron emission from electrons in a laser-wakefield accelerator has also been demonstrated [12], and show enhanced spacial and temporal resolution, with a limited photon flux compared to hard X-ray FELs.

The advent of hard X-ray Free Electron Lasers (XFELs) has overcome these limitations. The x-ray beam generated in an XFEL has a high spatial and temporal coherence, a short pulse duration (< 50 fs), narrow bandwidth (eV) and an extreme peak brightness (10^{33} photons s^{-1} mrad^{-2} mm^{-2} / 0.1 %BW [13]). Using these high-quality beams to image high energy density states has pushed the boundaries of spatial and temporal resolution, leading to discovery of never-seen-before phenomena that would not have been resolvable with optical backlighters otherwise. At the Matter at Extreme Conditions station at LCLS, the x-ray imaging platform [14, 15] has been used to probe shocks in diamond [16] and low density foams [17], the interplay of void in materials and shock propagation [18] and multi-frame imaging [19]. At SACLA, imaging has been used to elucidate electron transport dynamics in solid foils and nanowire arrays [20], shock splitting in diamond [21] and to elucidate turbulent spectra from Rayleigh-Taylor instabilities with unprecedented resolution [22]. At EuXFEL, a new pathway to achieve high-pressure states via convergent shockwaves was found in micrometer-sized wires [23].

X-ray imaging techniques are heavily dependant on the x-ray source. X-ray beams generated by laser backlighters have a larger energy bandwidth than those from synchrotron and XFELs. Free-propagating x-ray phase contrast imaging (XPCI) or radiography methods have performance less dependant on the polychromaticity of the source, while grating interferometric methods will suffer of reduced contrast because of the energy bandwidth. Furthermore, the divergence of the beam in a laser-based backlighter has enabled the probing of mm sized samples, something still to be demonstrated at an XFEL. A review and comparison between the usage of laser backlighters, synchrotron beams and XFEL beams applied to high-energy-density systems can be found in [24].

In this paper, we describe the experimental imaging platform developed at the High Energy Density - Helmholtz International Beamline for Extreme Fields (HED-HiBEF) instrument at EuXFEL [25]. We will discuss the technical aspects and the resolution limitations. We will show examples of physical processes generated with the high-intensity short-pulse laser, ReLaX [26], and the high-energy nanosecond-pulse laser DiPOLE-100X [27]. Finally, we examine the prospects of using this platform for fusion relevant research with the current capabilities at HED-HiBEF and when coupling it to a kJ-class laser.

2 The imaging platform at HED-HiBEF

The standard hard x-ray imaging setup at the HED-HiBEF instrument consists of a set of beryllium compound refractive lenses (CRLs) and a high-magnification optical microscope with a scintillator screen. The CRL sets are adapted to the x-ray energy as well as the desired magnification. The typical parameters of the CRLs are stacks of 15 to 34 lenses (each lens has a curvature radius of 50 µm and an aperture of 400 µm), with focal ranges covering 15 - 35 cm and magnification of 15-34. Up to now, the energy range covered has been from 7 keV to 8.5 keV; however, this can be extended to higher x-ray energies. The high-magnification detector consists of a scintillator (GAGG, Lu:Ce, YAG) coupled to a CMOS detector (Andor Zyla) via optical objectives with a selectable magnification of 2x, 7.5x and 10x [28]. The highest x-ray and optical magnification of 340 results in an equivalent pixel size on target down to 18.3 ± 0.1 nm based on calibrated target measurements.

The lenses are located at a distance after the target such that an image is formed on the scintillator downstream. The distance from the target to the detector is flexible ranging from 2 m to 6.3 m. The lenses are mounted on a hexapod to allow precise alignment of the stack in 6 degrees

of freedom. The hexapod is located on top of two linear stages, one transversal to the beam, for a quick switch of in and out lens position, and one longitudinal to the beam to scan along the x-ray axis. The usual travel range along the x-ray axis is about ±10 cm. This holder is compatible with either ReLaX or DiPOLE-100X beam routings (as shown in Figure 1, with the imaging CRL labeled CRL4b), as well as additional diagnostics like x-ray spectroscopy. Additionally, a twin CRL (CLR4a in Figure 1) stack can be placed in front of the target to generate a sub-micrometer focus on target, or use a point-projection imaging scheme. Both sets can be used simultaneously to measure the focal spot size, or monitor the overlap in experiments using the two-color XFEL mode. In this special mode, XFEL can deliver two pulses, separated up to 500 fs in time and up to a few hundred eV in energy. Overlap of the two pulses can be ensured by this imaging setup.

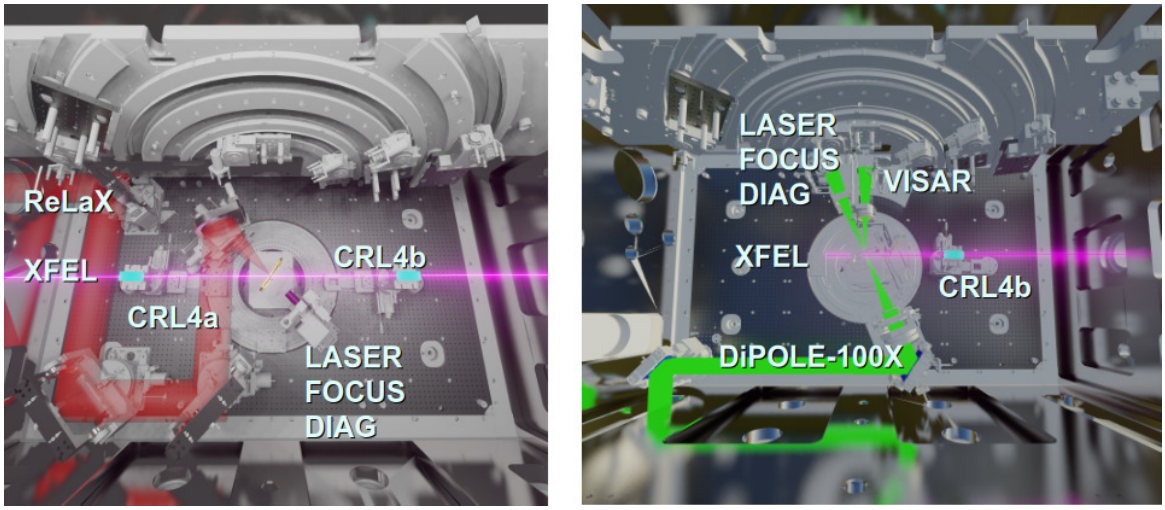

Figure 1. X-ray imaging setups: a) in combination with ReLaX and b) in combination with DiPOLE-100X. The detector is located outside the interaction chamber to the right in both images.

The intensity at the detector can be described via the transport of intensity equation [29]:

$$I(x,y,\Delta z) = I(x,y) - \frac{\Delta z}{k}\nabla\cdot[I(x,y)\nabla\Phi(x,y)] \tag{1}$$

with $I(x,y)$ the intensity in the plane at the object exit (what is known as 'contact plane'), Δz is the x-ray propagation distance from the target until the detector, k is the x-ray wave number and $\Phi(x,y)$ is the phase of the object. In this equation, the index of refraction $n = 1-\delta+i\beta$ of the object is encoded: the absorption is related to β since $I(x,y) = I_0 e^{(-2k\int\beta(x,y,z')dz')}$ and the phase is $\Phi = k\int\delta(x,y,z')dz'$, with the integration through the target thickness, along the x-ray axis. Therefore, it is possible to extract the object index of refraction under certain assumptions using phase-retrieval methods [30, 31, 32]. However, single-shot reconstruction of the object suffers in laser-plasma experiments from multiple issues: the uncertainty in the illumination function with variation in intensity and jitter, the plasma generated in the interaction and the non-uniformities introduced by the CRLs can affect the convergence of the reconstruction methods.

Most of the problems previously mentioned can be mitigated and the sensitivity of the system enhanced by means of Talbot-Lau interferometry. This technique has been successfully employed at laser facilities with x-ray backlighters [33, 34, 35, 36] and other XFELs [37, 17, 15]. Talbot-Lau interferometry is based on the Talbot effect. To record the interferometric data, a detector is placed in an arbitrarily chosen self image Talbot plane. Disturbance of the interferometric pattern by the introduction of a sample in the x-ray path can thereafter be linked to transmission, differential phase, and dark field radiographs through Fourier analysis [38].

In a more formal way, the intensity at the detector can be expressed as [33, 34]:

$$I(x,y) = A(x,y) + B(x,y)e^{i\phi(x,y)} \tag{2}$$

where $A(x,y)$, $B(x,y)$ and $\phi(x,y)$ are real functions that can be extracted and related to the attenuation, the fringe visibility and the phase. A Fourier analysis using an image with the object and an image without the object allows the extraction of the object properties as attenuation $A = A_{obj}/A_{ref}$ and $\phi = \phi_{obj} - \phi_{ref}$. In this case, the problem has shifted from analyzing the target image itself, to analyzing the variations on the periodicity and amplitude of the grating peaks,

without any assumption on the object itself. The grating used in our case is a checkerboard diamond grating with a phase shift of $\pi/2$ at 8 keV, horizontal pitch of 9.2 µm and thickness of 10 µm.

It is important to note, that the excellent quality of the XFEL source is responsible for obtaining high-quality Talbot-Lau interferometric images. In particular, the fringe contrast will decrease in the case of a laser backlighter, and therefore the subsequent reconstructed physical quantities will have larger uncertainties. Furthermore, phase reconstruction, be it either with phase retrieval or Talbot-Lau interferometry, is not the only path towards obtaining a physical understanding from the x-ray images. For example, matching synthetic x-ray profiles from simulations with experimental data it is possible to extract the shock front shape as well as density as demonstrated in [6] under strong shock regime. Using refraction enhanced radiography the fuel-ablator interface acceleration has been measured [39]. Since laser backlighter x-ray sources do not typically rely on CRL-based imaging optics (like synchrotrons and XFELs), avoiding CRL-induced aberrations, and therefore they benefit the most from these techniques.

The resolution of the imaging system was measured using a calibration target (XRESO-50HC from NTT). It consists of a Siemens Star made of tungsten with a thickness of 500 nm. The minimum spatial features are 50 nm at the centermost part of the patterned area. Figure 2 shows the flatfielded data, using the XPCI configuration (without phase retrieval), of such a calibration target. Sub-500 nm structures are resolved for the highest magnification configuration.

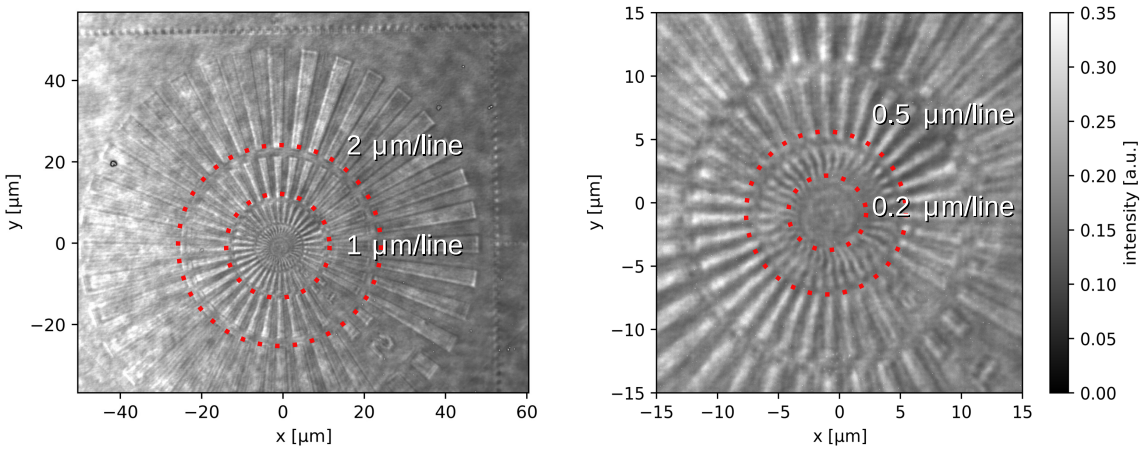

Figure 2. Flatfielded data of a resolution target for x-ray imaging. The circular areas show the dimensions of each individual line at that radius.

3 Imaging results examples

Here we showcase a series of examples of the phenomena that have been investigated with these techniques.

3.1 Blast waves generated with a short-pulse laser

The high-intensity short-pulse interaction with the target generates a hot spot of the order of a few micrometers. The high temperature gradient between this spot and the surrounding material leads to the generation of a blast wave. Previous studies of isochorically heated solids have characterized the hot electron source as well as the preheating and velocity of the wave [40, 41, 42]. They have also used simulations to infer the shock pressures in the range of 100 Mbar. Imaging of blast waves has also been performed at MEC [15]. The high energy density states generated in this fashion show great promise towards the study of astrophysical phenomena in the laboratory.

The platform was used in combination with ReLaX to study shocks propagating in wire targets. Here, we show a comparison between XPCI and Talbot-Lau imaging on aluminium wires of 25 μm. In Figure 3, we show both the reconstructed phase for an undriven target, as well as the interaction of ReLaX and the target.

In the case of XPCI (displayed in Figure 3 a), the x-ray magnification was $M_x = 15$ and the detector optical magnification $M_o = 2$, corresponding to a total magnification of 30 and an equivalent pixel size on target of 216 nm/px. We use a non-linear phase-retrieval algorithm in the near-field regime with Tikhonov regularization [32] as implemented in the *HoToPy* package for python [43]. The constraints used were a single element object (aluminium) with a

$\beta/\delta = 1.63 \times 10^{-3}$, a support indicating where the object was located and a non-positive phase. The Fresnel number for this configuration was $Fr = 0.012$. With these settings, the reconstructed phase shift for the aluminium wire at the center is 8.3 rad.

In the case of Talbot-Lau imaging, the x-ray magnification was $M_x = 34$ and the detector magnification $M_o = 10$. The total magnification was 340 with an equivalent pixel size on target of 18 nm/px. The phase was retrieved using the TIA/TNT algorithm [38]. The data shown here correspond to a shot with a pump-probe delay of 0 ps. Essentially, the areas away from the laser focus still remain at cold temperature and no hydrodynamic motion has taken place yet. A lineout comparison between both phase retrieval methods and with the phase shift expected from a perfect aluminium wire is shown in panel c) showing a good agreement between the methods.

The differences between both imaging techniques become clear when studying blast waves generated by the ReLaX interaction with the target. For the XPCI case, the recorded signal around the shock region contains a mixture of the imaging of CRL impurities together with the plasma halo. These features cannot be correctly phase-retrieved. Furthermore, the shock phase-shift obtained is lower than that of cold aluminium. This limitation can be overcome by using Talbot-Lau imaging. Using the Talbot grating as an interferometer, effectively provides a filter that compensates spurious effects not related to the object imaging. This can be seen on how the Talbot-Lau phase maps are more homogeneous across the whole wire when compared to the XPCI phase. A lineout along the central part of the shock is shown in panel f). The correct phase projection is retrieved and an increased phase-shift shows the location of the shock front.

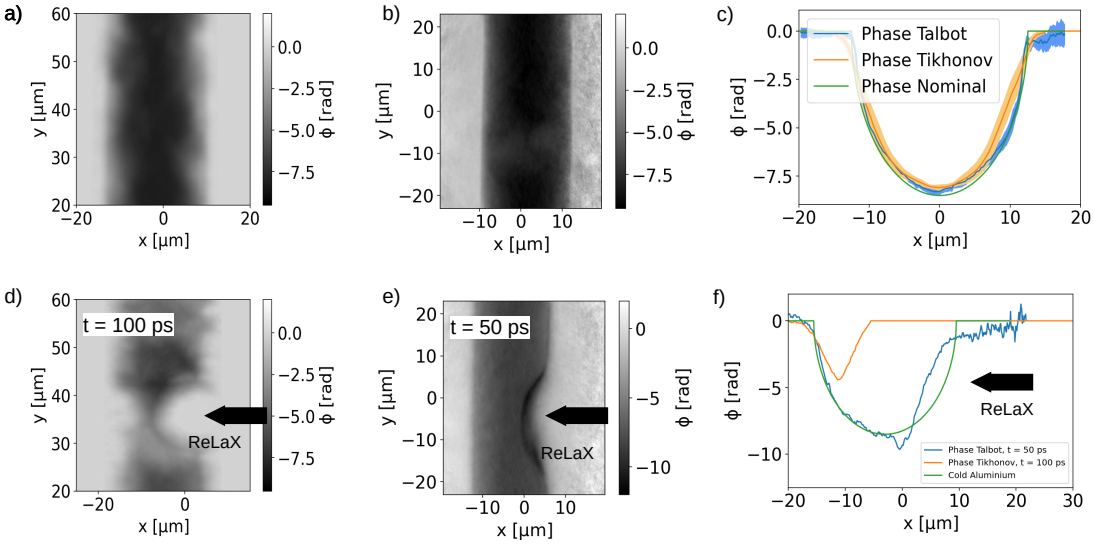

Figure 3. Retrieved phase for aluminium wires. For XPCI configuration: a) x-ray only imaging of the unpumped wire, d) x-ray imaging 100 ps after ReLaX arrival. For Talbot-Lau imaging configuration: b) x-ray only for cold aluminium wire, e) Talbot-Lau imaging 50 ps after ReLaX arrival. Panel c) shows a lineout at the central part of the both XPCI and Talbot-Lau configuration images and the expected theoretical phase shift from a perfect 25 μ aluminium wire. Panel f) shows a horizontal lineout at the central part of the shock for both cases. In the lower panels the thick black arrow represents the projected incoming direction of ReLaX in the x-ray imaging plane.

We emphasize that the outcome of this comparison is heavily biased by the source itself. As mentioned before, the narrow bandwidth of the XFEL beam is beneficial to the Talbot-Lau method. At the same time, the use of x-ray optics is detrimental to the XPCI method due to aberrations. Laser backlighters provide complementary properties, i.e. a wider bandwith but a more homogeneous illumination when compared to the XFEL beam at HED-HiBEF. In that case, XPCI, while having worse spatial resolution, provides results with enough quality as to extract information, in a quantitative way, without the need of phase retrieval methods.

3.2 Wire compression driven by return currents

The first implementation of the imaging platform with ReLaX enabled the discovery of a compression wave in micrometer-thin wires [23]. Follow-up experiments have demonstrated the robustness of this compression method by using different materials [44]. In this process, the hot

electrons expelled from the target generate a charge imbalance that drives an intense return current. This return current lasts in the order of the laser pulse duration and is restricted to a skin depth of less than 1 µm. This surface is heated to high temperatures, up to hundreds of eV. The gradient of the surface temperature to the colder inner material leads to an ablation driven cylindrical wave that travels towards the wire axis. At the convergence point of the wave, a 10x compression has been demonstrated with simulations predicting pressures up to 800 Mbar on copper [23].

Here we show results of the compression of a 25 µm aluminium wire with Talbot-Lau imaging for the first time. The phase retrieval for a cold wire is displayed in the upper part of Figure 4 a), while the phase shift for a pump-probe delay of 700 ps is shown in the lower panel. For this delay, the compression wave reached the wire axis at a distance of approximately 45 µm. The phase retrieved image was Abel inverted using a deconvolution procedure developed by Daun et al. [45] and implemented in the *pyabel* package. The density shown on panel b) exhibits a maximum at the wire axis after an abel inversion, corresponding to a density $\rho = 12.7\,\mathrm{g\,cm^{-3}}$. This calculated compression factor is 4.7.

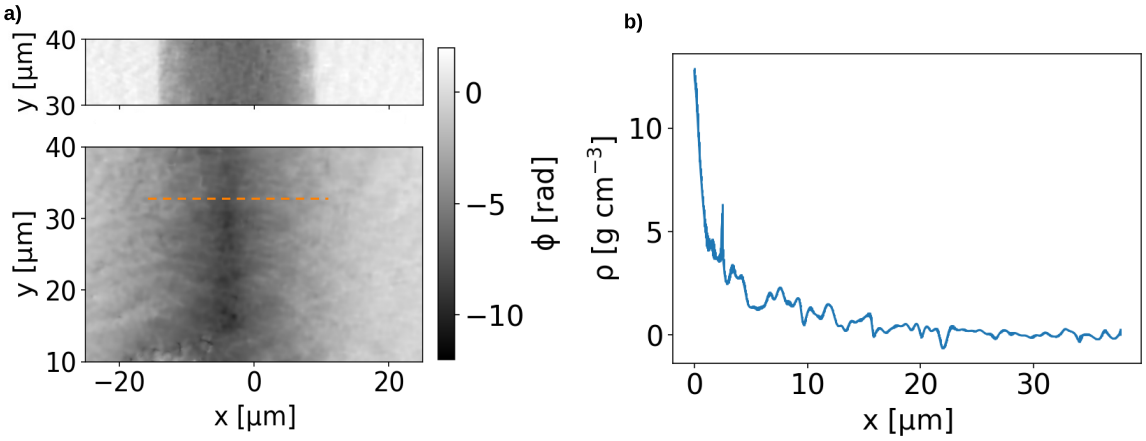

Figure 4. a) Phase maps for an aluminium wire, with the upper panel showing the cold target and the lower panel the target 700 ps after ReLaX arrival. The orange dashed line indicates the point along the wire where the compression is maximal. b) Abel inverted density at the highest compression point.

3.3 Charge-state specific resonant imaging

The narrow energy bandwidth of the XFEL beam enables investigations of energy-selective process. In particular, specific electron transitions between the K and L shells can be probed by using ReLaX to ionize the target and using the XFEL beam to excite the electrons. In our case, copper foils with thickness of 2 µm and 5 µm were used as targets. We chose an XFEL energy of 8.163 keV, corresponding to the energy transition from the K-shell to the L-shell of Cu^{21+} ions. Previous experiments have performed studies of resonant absorption with spectroscopy and x-ray imaging [46, 47].

The flatfielded image, in the XPCI configuration, of a 5 µm thick copper foil upon ReLaX irradiation can be seen in Figure 5 a). The delay between ReLaX and X-ray was 200 fs. A decrease in detector counts at the center of the image, with a width comparable to the laser focus is apparent at the center of the image. However, this attenuation is a mixture of absorption and refraction effects. Deconvolving the actual attenuation would require making an assumption, a priori, on the β/δ ratio for copper. As this is a resonant process, the value of β is highly dependent on the ionization state of the copper foil. The ionization state itself is not spatially homogeneous, adding further complications to any phase-retrieval attempt. In the case of Talbot-Lau imaging, without assumptions on the target itself, the situation is different. Here we show the first application of Talbot-Lau imaging to a charge-state resonant absorption process with an example of the transmission map and phase map for a pump-probe delay of 4.8 ps. Figure 5 b) and c) show the reconstructed maps. The phase shift displayed corresponds to the phase delay with respect to a cold copper foil, thus a null phase shift is shown across the area with a deviation where the laser impacted on the foil. Similarly, the transmission map shows the transmission with respect to a cold foil. There is an ambiguity due to the XFEL pulse energy used to measure the cold foil and the laser-shot foil. To account for this, we use a relative measurement of the transmission between the laser irradiated area, and an area far outside. This ratio of transmitted x-rays inside the laser area to outside is 0.3. If the effect were to be volumetric through the complete foil thickness, the mass

attenuation coefficient would be 613 cm^2 g^{-1}. For a cold foil of the same thickness, the mass attenuation coefficient at this x-ray energy is 48 cm^2 g^{-1}. This is a clear indication that the x-rays are being resonantly absorbed.

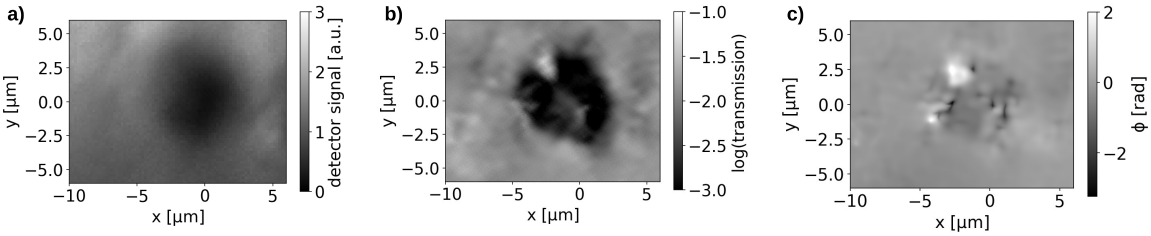

Figure 5. a) Flatfielded x-ray image of a 5 µm copper foil, 200 fs after ReLaX arrival. b) Attenuation map for a 2 µm copper foil 4.8 ps after ReLaX main pulse. c) Phase map for the same 2 µm foil and time step.

3.4 Shock-compression of polystyrene with DiPOLE-100X

Shock compression is a standard technique to study high-pressure states and phase transitions. Most shock compression studies employ x-ray diffraction and velocity interferometer system for any reflector (VISAR) techniques to extract the conditions reached during compression. However, in the case of VISAR, a limitation is given in the shock conditions that can be studied due to the reflectivity needed as well as the impossibility of probing shocks during propagation inside optically opaque targets.

Employing imaging to study the propagation of a laser generated shock in a material extends the conditions to be studied, and provides snapshots of the shock development during and after laser irradiation. We used a target made of polystyrene, with an aluminium ablator deposited on one face. The polystyrene block had dimensions $0.475 \times 0.475 \times 5$ mm^3, the aluminium ablator was $0.475 \times 0.010 \times 5$ mm^3. The DiPOLE laser shot on the ablator side at an angle of 22.5° with respect to the target normal, launching a shock through the aluminium and polystyrene materials. The x-ray probed transversally to the shock propagation. DiPOLE was used at 2ω (515 nm), with 35 J on target and a phase plate of 300 µm. The Talbot-Lau technique was used for x-ray imaging, similar to [15].

The phase retrieved image in Figure 6 a) shows the richness of the shock process. The phase is calculated with respect to the undriven target. The ablator is seen in the area $x < -20$ µm. The shock front appears in the range of $12 < x < 16$ µm. There, we observe the presence of at least two distinct discontinuities in the phase. This example shows the enhanced capabilities of imaging shocks against other methods: the possibility to observe the shock front, and possibly rarefaction waves as they propagate inside the target. Recent theoretical studies have analyzed the assumptions and effect of an ablator thickness and impedance mismatch in laser-loading experiments [48]. Such theoretical studies could obtain experimental validation with this imaging platform.

4 Research potential for IFE applications

Currently, a demonstration of a target gain > 1 has only been demonstrated at the NIF [49]. This achievement was the culmination of decades of improvements in laser design, targetry, diagnostics and simulations. An overview of the challenges overcome can be found in [50, 51].

The conditions needed to reach ignition are extreme, thus an implosion facility needs the most energetic laser available such as NIF and LMJ. However, on the path to ignition and inertial fusion energy, challenges can be tackled with smaller lasers, currently available at XFEL facilities. For example, inhomogeneities in the ablator can lead to degradation in performance [52]. Studies performed at MEC and HED-HiBEF have demonstrated diamond formation from plastic ablators, similar to those used in NIF capsules, when irradiated with a long pulse laser [53, 54]. Hydrodynamic instability control has been, and remains, a challenge. The ability to observe the instability growth holds great promise towards a more effective suppression. Studies of instabilities and turbulent regime have been performed at SACLA [22]. New nano-accelerator concepts are also gaining momentum, such as nanowire arrays for direct drive laser fusion. Experiments aimed to understanding nanowire evolution under irradiation have been started [20].

The inherent value of performing imaging experiments is apparent. However, it is not the only technique available at XFEL facilities. Other methods for probing plasmas can complement imaging: small-angle x-ray scattering can be used to study kinetic instabilities and blast waves with nanometer scale resolution [55, 56, 57, 58], grazing incidence small-angle x-ray scattering

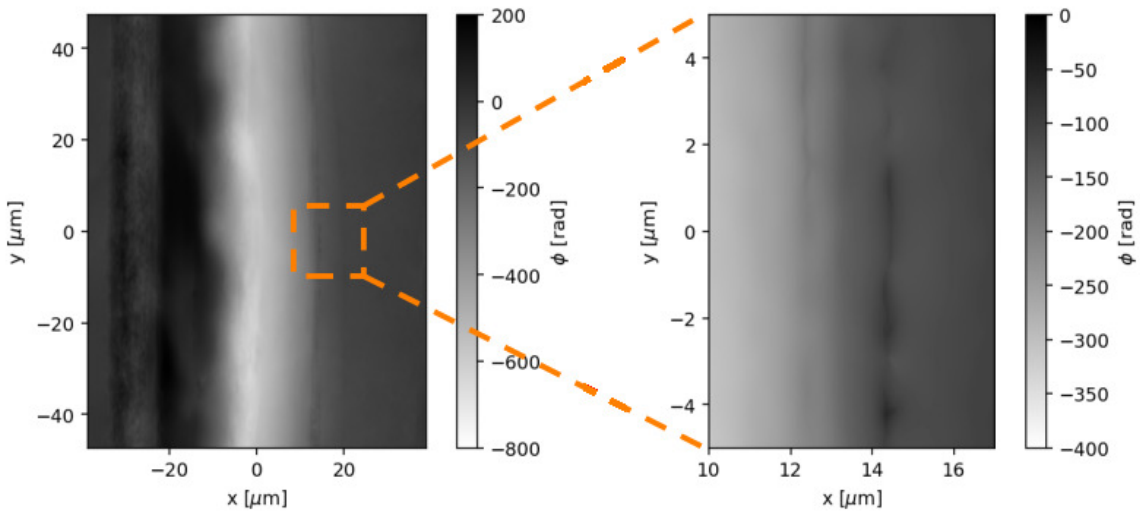

Figure 6. Left: Phase shift map for a shocked polystyrene block with respect to an unshocked block. Right: zoom in section around the front shock showing multiple phase sharp gradients.

provides information on surface structures [59, 60, 61], x-ray Thomson scattering accesses temperature and collective phenomena [62, 63, 64, 65], diffraction is a standard diagnostic to study phase transitions and material deformation under high-strain [66, 67, 68], among others.

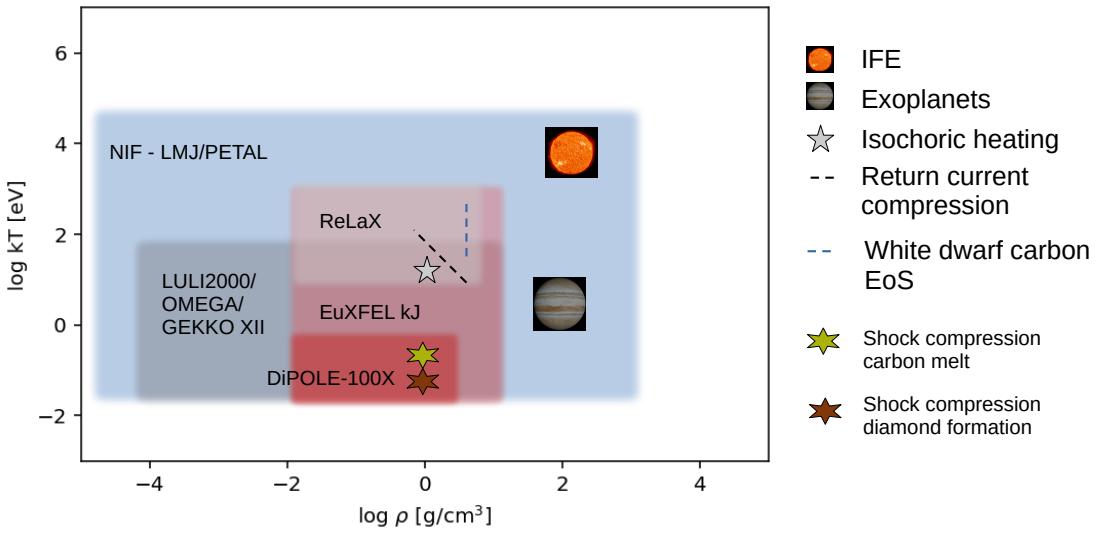

Figure 7. Illustration of the phase map for carbon and hydrocarbon materials covered by different laser facilities. IFE shows the implosion point achieved at NIF in 2022 [49]. Exoplanets. Isochoric heating of plastic materials [69]. Return current driven cylindrical compression [23]. Carbon equation-of-state measurement at white dwarf conditions [70]. Carbon melting and phase-coexistence [71]. Diamond formation from hydrocarbons [53].

Finally, it is of interest to discuss the potential of XFELs when coupled to higher-intensity and higher-energy lasers. A workshop designed to identify the science that can be addressed at the European XFEL took place in 2024 [72] with a follow-up in 2025. Within the German Fusion Action Plan as part of the High Tech Agenda Germany, the possibility of installing a kJ-class laser and a petawatt short-pulse laser at the European XFEL is under consideration.

To provide an overview as to what science cases could be achieved with such a facility, we compare the conditions achievable at HED-HiBEF with other lasers used for IFE research in Figure 7. There the conditions achieved for an indirect drive ignition are represented by the "IFE" point [49], only reachable by Mega-Joule lasers. Other experiments at NIF studied the carbon equation of state in conditions relevant to white dwarf envelopes [70]. While temperatures of keV are

achievable with short pulse lasers, the relevant compression factor is not. Cylindrical compression of wires has shown to reach a compression of 10x in copper, and is expected to reach similar compression for hydrocarbons, the temperature at the convergence point is of 10s eV, lower than the one achieved at NIF ∼100 eV [70]. Isochoric heating studies of plastics in reduced mass targets was investigated with Gekko MII [69], at intensities $10^{17} - 10^{18}$ W cm^{-2}, below the maximum achievable intensity at ReLaX 10^{21} W cm^{-2}. In planar shocks, the study of liquid carbon was done at HED-HiBEF with DiPOLE-100X [71], while the original diamond formation in shock compressed hydrocarbons was performed at the MEC station [53].

A kJ-class laser would increase the pressure range currently achievable with DiPOLE-100X from ∼1.5 Mbar, to 10-20 Mbar, and the combination with the XFEL beam would open the path to exploring such states with unprecedented spatial and temporal resolution. At the same time, a short-pulse high-intensity petawatt laser is also considered. This would open the possibility to full equation of state measurements via a combination of imaging and x-ray Thomson scattering, extending existing equation of state measurements, for example in the case of plastic foams [73], or providing complementary precision measurements for high-density carbon (HDC) ablators [74, 75] beyond the current limitations of VISAR techniques. As shown in section 3.3, the XFEL beam energy can be tuned to K-shell to L-shell transitions. Resonant imaging would track the evolution of ablators and material mixing with high-spatial and temporal resolution as well as temperature resolved measurements (by shifting the XFEL energy across different resonances) by means of dopants in the target acting as tracers [76]. The imaging of instabilities has already been mentioned; however, a combination of small-angle x-ray scattering together with imaging, would allow the measurement of instabilities and shocks (and shock front gradient) with spatial scales from nm to µm [77].

5 Conclusions

In this paper, we have introduced the hard x-ray imaging platform developed at HED-HiBEF. We have shown the setups combining it together with the ReLaX and DiPOLE-100X drivers. Thanks to the high-quality properties of the XFEL beam, with its high brilliance, the high spatial and temporal coherence, and narrow bandwidth, we demonstrate the applicability of the Talbot-Lau imaging method as well as the limitations of phase retrieval methods due to the aberrations introduced by the x-ray optics. The platform has a spatial resolution better than 500 nm and a temporal resolution better than 50 fs, in contrast to the typical resolution of tens of µm (depending on geometry and detector configuration) achieved with laser backlighters. We have compared the performance of magnified x-ray imaging and Talbot-Lau imaging, showing the advantages of the latter while investigating blast waves and cylindrical compression in aluminium wires with the ReLaX laser. Tuning the XFEL energy to a resonant energy with a specific electronic transition, an increase of the opacity induced by the transition of electrons from the K-shell to the L-shell has been observed, providing a diagnostic of the plasma state with specific conditions. An application to imaging of planar shocks with DiPOLE-100X has been discussed, showcasing the spatial sensitivity to probe intricacies of shock front generation and propagation. We have also discussed the complementarity of this technique with other x-ray methods available at HED-HiBEF and have shown some of the science cases related to fusion that could be addressed with a kJ-class laser coupled to the XFEL beam.

The next steps for improving the x-ray imaging quality are focused in reducing the aberrations introduced by the compound refractive lenses. Alternative materials for the lenses are under investigation, like SU8 and diamond materials. We not, however, that for the x-ray energies used in the experiments described in this manuscript, alternative CRL materials result in a lower numerical aperture and transmission. Complementary, the use of Fresnel Zone Plates is under study.

Acknowledgments

We thank the European XFEL in Schenefeld, Germany, and the HiBEF user consortium for the provision of X-ray laser time at the HED-HiBEF scientific instrument under proposal numbers 5689, as part of the HiBEF priority access, 4597 and 9796, and thank their staff for their support and the equipment provided to make this experiment possible. We thank Dr. Steve Gales from AWE for the provision of the polystyrene rod targets.

Funding

This work was partially supported by the Center for Advanced Systems Understanding (CASUS), financed by Germany's Federal Ministry of Education and Research (BMBF) and the Saxon state government out of the State budget approved by the Saxon State Parliament. This work has

received funding from the European Union's Just Transition Fund (JTF) within the project *Röntgenlaser-Optimierung der Laserfusion* (ROLF), contract number 5086999001, co-financed by the Saxon state government out of the State budget approved by the Saxon State Parliament. Tobias Dornheim gratefully acknowledges funding from the Deutsche Forschungsgemeinschaft (DFG) via project DO 2670/1-1. The work of G. P.-C. has been supported by Research Grant No. PID2022-137632OB-I00 from the Spanish Ministry of Science and Innovation. The ELI-NP team acknowledges IFA (Institute of Atomic Physics, Romania) projects ELI-RO/RDI/2024_028 FLIGHT, ELI-RO/RDI/2024_016 DELPHI, and ELI-RO/RDI/2024_021 LGS.

Author contributions

A. L. G., M. M., V. B., T. T., B. N. designed the experiment. A. L. G., G. P.-C. and M.-L. H. analysed the data, A. L. G., M. M., V. B., P. V. G., M.-L. H., H. H., M. J., J. L., J.-P. N., Q. N., C. B. Q., S. V. R., L. R., A. R.-F., C. S., J. S., M. T., P. V., T. T., K. A., C. B., E. B., M. C., D. D., N. F., T. G., S. G., J. H., L. H., O. S. H., T. K., H. J. L., M. M., B. N., M. N., A. P., T. R. P., M. R., M. S., M. V. and L. Y. performed the experiments. T. T. and A. L. G. supervised the project. All authors reviewed the manuscript.

Data availability

Data recorded for the experiment at the European XFEL are available at doi:10.22003/XFEL.EU-DATA-005689-00, doi:10.22003/XFEL.EU-DATA-004597-00, and doi:10.22003/XFEL.EU-DATA-009796-00.

References

[1] Landen OL, Farley DR, Glendinning SG, Logory LM, Bell PM, Koch JA, et al. X-ray backlighting for the National Ignition Facility (invited). Review of Scientific Instruments. 2001 01;72(1):627-34. Available from: https://doi.org/10.1063/1.1315641.

[2] Barrios MA, Regan SP, Fournier KB, Epstein R, Smith R, Lazicki A, et al. X-ray area backlighter development at the National Ignition Facility (invited)a). Review of Scientific Instruments. 2014 08;85(11):11D502. Available from: https://doi.org/10.1063/1.4891713.

[3] Turk G, Reverdin C, Gontier D, Darbon S, Dujardin C, Ledoux G, et al. Development of an x-ray imaging system for the Laser Megajoule (LMJ)a). Review of Scientific Instruments. 2010 10;81(10):10E509. Available from: https://doi.org/10.1063/1.3475788.

[4] Marshall FJ, Ivancic ST, Mileham C, Nilson PM, Ruby JJ, Stoeckl C, et al. High-resolution x-ray radiography with Fresnel zone plates on the University of Rochester's OMEGA Laser Systems. Review of Scientific Instruments. 2021 03;92(3):033701. Available from: https://doi.org/10.1063/5.0034903.

[5] Bouffetier V, Pérez-Callejo G, Stutman D, Stoeckl C, Begishev IA, Theobald W, et al. Referenceless, grating-based, single shot X-ray phase contrast imaging with optimized laser-driven K-α sources. Opt Express. 2024 Sep;32(20):34694-709. Available from: https://opg.optica.org/oe/abstract.cfm?URI=oe-32-20-34694.

[6] Antonelli L, Atzeni S, Schiavi A, Baton SD, Brambrink E, Koenig M, et al. Laser-driven shock waves studied by x-ray radiography. Phys Rev E. 2017 Jun;95:063205. Available from: https://link.aps.org/doi/10.1103/PhysRevE.95.063205.

[7] Rigon G, Albertazzi B, Mabey P, Michel T, Falize E, Bouffetier V, et al. Exploring the Atwood-number dependence of the highly nonlinear Rayleigh-Taylor instability regime in high-energy-density conditions. Phys Rev E. 2021 Oct;104:045213. Available from: https://link.aps.org/doi/10.1103/PhysRevE.104.045213.

[8] Antonelli L, Theobald W, Barbato F, Atzeni S, Batani D, Betti R, et al. X-ray phase-contrast imaging of strong shocks on OMEGA EP. Review of Scientific Instruments. 2024 11;95(11):113504. Available from: https://doi.org/10.1063/5.0168059.

[9] Tommasini R, Field JE, Hammel BA, Landen OL, Haan SW, Aracne-Ruddle C, et al. Tent-induced perturbations on areal density of implosions at the National Ignition Facilitya). Physics of Plasmas. 2015 05;22(5):056315. Available from: https://doi.org/10.1063/1.4921218.

[10] Wegert L, Schreiner S, Rauch C, Albertazzi B, Bleuel P, Fröjdh E, et al. Demonstrating grating-based phase-contrast imaging of laser-driven shock waves. Matter and Radiation at Extremes. 2024 06;9(4):047803. Available from: https://doi.org/10.1063/5.0200440.

[11] Do A, Angulo AM, Hall GN, Nagel SR, Izumi N, Kozioziemski BJ, et al. X-ray imaging of Rayleigh–Taylor instabilities using Fresnel zone plate at the National Ignition Facility. Review of Scientific Instruments. 2021 05;92(5):053511. Available from: https://doi.org/10.1063/5.0043682.

[12] Wood JC, Chapman DJ, Poder K, Lopes NC, Rutherford ME, White TG, et al. Ultrafast Imaging of Laser Driven Shock Waves using Betatron X-rays from a Laser Wakefield Accelerator. Scientific Reports. 2018 Jul;8(1):11010. Available from: https://doi.org/10.1038/s41598-018-29347-0.

[13] Tschentscher T, Bressler C, Grünert J, Madsen A, Mancuso AP, Meyer M, et al. Photon Beam Transport and Scientific Instruments at the European XFEL. Applied Sciences. 2017;7(6). Available from: https://www.mdpi.com/2076-3417/7/6/592.

[14] Nagler B, Schropp A, Galtier EC, Arnold B, Brown SB, Fry A, et al. The phase-contrast imaging instrument at the matter in extreme conditions endstation at LCLS. Review of Scientific Instruments. 2016 10;87(10):103701. Available from: https://doi.org/10.1063/1.4963906.

[15] Galtier E, Lee HJ, Khaghani D, Boiadjieva N, McGehee P, Arnott A, et al. X-ray microscopy and talbot imaging with the matter in extreme conditions X-ray imager at LCLS. Scientific Reports. 2025 Mar;15(1):7588. Available from: https://doi.org/10.1038/s41598-025-91989-8.

[16] Schropp A, Hoppe R, Meier V, Patommel J, Seiboth F, Ping Y, et al. Imaging Shock Waves in Diamond with Both High Temporal and Spatial Resolution at an XFEL. Scientific Reports. 2015 Jun;5(1):11089. Available from: https://doi.org/10.1038/srep11089.

[17] Parisuaña C, Valdivia MP, Bouffetier V, Kurzer-Ogul K, Pérez-Callejo G, Bott-Suzuki S, et al. Shock propagation in aerogel and TPP foams for inertial fusion energy target design. Physics of Plasmas. 2025 08;32(8):082707. Available from: https://doi.org/10.1063/5.0273572.

[18] Hodge DS, Leong AFT, Kurzer-Ogul K, Pandolfi S, Montgomery DS, Shang J, et al. Single-shot in-line x-ray phase-contrast imaging of void-shockwave interactions in fusion energy materials. Physics of Plasmas. 2025 08;32(8):083903. Available from: https://doi.org/10.1063/5.0272820.

[19] Hodge DS, Leong AFT, Pandolfi S, Kurzer-Ogul K, Montgomery DS, Aluie H, et al. Multi-frame, ultrafast, x-ray microscope for imaging shockwave dynamics. Opt Express. 2022 Oct;30(21):38405-22. Available from: https://opg.optica.org/oe/abstract.cfm?URI=oe-30-21-38405.

[20] Tanaka D, Sawada H, Idesaka T, Nakatsuji C, Matsuura S, Sato T, et al. Experimental investigation on nanowire array irradiated with ultrahigh intensity laser at x-ray free electron laser facility SACLA: Fabrication of nanowire array target and its application to ultrafast time-resolved measurements. Journal of Applied Physics. 2025 03;137(12):125901. Available from: https://doi.org/10.1063/5.0251649.

[21] Makarov S, Dyachkov S, Pikuz T, Katagiri K, Nakamura H, Zhakhovsky V, et al. Direct imaging of shock wave splitting in diamond at Mbar pressure. Matter and Radiation at Extremes. 2023 09;8(6):066601. Available from: https://doi.org/10.1063/5.0156681.

[22] Rigon G, Albertazzi B, Pikuz T, Mabey P, Bouffetier V, Ozaki N, et al. Micron-scale phenomena observed in a turbulent laser-produced plasma. Nature Communications. 2021 May;12(1):2679. Available from: https://doi.org/10.1038/s41467-021-22891-w.

[23] Laso Garcia A, Yang L, Bouffetier V, Appel K, Baehtz C, Hagemann J, et al. Cylindrical compression of thin wires by irradiation with a Joule-class short-pulse laser. Nature Communications. 2024 Sep;15(1):7896. Available from: https://doi.org/10.1038/s41467-024-52232-6.

[24] Montgomery DS. Invited article: X-ray phase contrast imaging in inertial confinement fusion and high energy density research. Review of Scientific Instruments. 2023 02;94(2):021103. Available from: https://doi.org/10.1063/5.0127497.

[25] Zastrau U, Appel K, Baehtz C, Baehr O, Batchelor L, Berghäuser A, et al. The High Energy Density Scientific Instrument at the European XFEL. Journal of Synchrotron Radiation. 2021 Sep;28(5):1393-416. Available from: https://doi.org/10.1107/S1600577521007335.

[26] Laso Garcia A, Höppner H, Pelka A, Bähtz C, Brambrink E, Di Dio Cafiso S, et al. ReLaX: the Helmholtz International Beamline for Extreme Fields high-intensity short-pulse laser driver for relativistic laser–matter interaction and strong-field science using the high energy density instrument at the European X-ray free electron laser facility. High Power Laser Science and Engineering. 2021;9:e59. E59. Available from: https://www.cambridge.org/core/product/2E9CD2B2288414E5785888C2354B3E7E.

[27] Mason P, Banerjee S, Smith J, Butcher T, Phillips J, Höppner H, et al. Development of a 100 J, 10 Hz laser for compression experiments at the High Energy Density instrument at the European XFEL. High Power Laser Science and Engineering. 2018;6:e65.

[28] Koliyadu JCP, Moško D, Asimakopoulou EM, Bellucci V, Birnšteinová Š, Bean R, et al. Development of MHz X-ray phase contrast imaging at the European XFEL. Journal of Synchrotron Radiation. 2025 Jan;32(1):17-28. Available from: https://doi.org/10.1107/S160057752400986X.

[29] TEAGUE MR. Irradiance moments: their propagation and use for unique retrieval of phase [Article]. J OPT SOC AM. 1982;V 72(N 9):1199 – 1209. Cited by: 237. Available from: https://www.scopus.com/inward/record.uri?eid=2-s2.0-0020178653&doi=10.1364%2fjosa.72.001199&partnerID=40&md5=b5ef1c182341197ffbaf7cc95e9e168a.

[30] Paganin D, Mayo SC, Gureyev TE, Miller PR, Wilkins SW. Simultaneous phase and amplitude extraction from a single defocused image of a homogeneous object. Journal of Microscopy. 2002;206(1):33-40. Available from: https://onlinelibrary.wiley.com/doi/abs/10.1046/j.1365-2818.2002.01010.x.

[31] Paganin DM, Favre-Nicolin V, Mirone A, Rack A, Villanova J, Olbinado MP, et al. Boosting spatial resolution by incorporating periodic boundary conditions into single-distance hard-x-ray phase retrieval. Journal of Optics. 2020 oct;22(11):115607. Available from: https://doi.org/10.1088/2040-8986/abbab9.

[32] Huhn S, Lohse LM, Lucht J, Salditt T. Fast algorithms for nonlinear and constrained phase retrieval in near-field X-ray holography based on Tikhonov regularization. Opt Express. 2022 Aug;30(18):32871-86. Available from: https://opg.optica.org/oe/abstract.cfm?URI=oe-30-18-32871.

[33] Valdivia MP, Stutman D, Stoeckl C, Mileham C, Begishev IA, Bromage J, et al. Talbot–Lau x-ray deflectometry phase-retrieval methods for electron density diagnostics in high-energy density experiments. Appl Opt. 2018 Jan;57(2):138-45. Available from: https://opg.optica.org/ao/abstract.cfm?URI=ao-57-2-138.

[34] Bouffetier V, Ceurvorst L, Valdivia MP, Dorchies F, Hulin S, Goudal T, et al. Proof-of-concept Talbot–Lau x-ray interferometry with a high-intensity, high-repetition-rate, laser-driven K-alpha source. Appl Opt. 2020 Sep;59(27):8380-7. Available from: https://opg.optica.org/ao/abstract.cfm?URI=ao-59-27-8380.

[35] Valdivia MP, Stutman D, Stoeckl C, Theobald W, Collins I G W, Bouffetier V, et al. Talbot-Lau x-ray deflectometer: Refraction-based HEDP imaging diagnostic. Review of Scientific Instruments. 2021 06;92(6):065110. Available from: https://doi.org/10.1063/5.0043655.

[36] Pérez-Callejo G, Bouffetier V, Ceurvorst L, Goudal T, Klein SR, Svyatskiy D, et al. Phase imaging of irradiated foils at the OMEGA EP facility using phase-stepping X-ray Talbot–Lau deflectometry. High Power Laser Science and Engineering. 2023;11:e49. E49. Available from: https://www.cambridge.org/core/product/53AEE63F6918AF67A9FFA2C23C5377A8.

[37] Bouffetier V. Développement de l'interférométrie X et application à l'imagerie par contraste de phase de plasmas denses et turbulents [Theses]. Université de Bordeaux; 2021. Available from: https://theses.hal.science/tel-03634981.

[38] Pérez-Callejo G, Bouffetier V, Ceurvorst L, Goudal T, Valdivia MP, Stutman D, et al. TIA: A forward model and analyzer for Talbot interferometry experiments of dense plasmas. Physics of Plasmas. 2022 04;29(4):043901. Available from: https://doi.org/10.1063/5.0085822.

[39] Do A, Weber CR, Dewald EL, Casey DT, Clark DS, Khan SF, et al. Direct Measurement of Ice-Ablator Interface Motion for Instability Mitigation in Indirect Drive ICF Implosions. Phys Rev Lett. 2022 Nov;129:215003. Available from: https://link.aps.org/doi/10.1103/PhysRevLett.129.215003.

[40] Jakubowska K, Batani D, Feugeas JF, Forestier-Colleoni P, Hulin S, Nicolaï P, et al. Generation of high pressures by short-pulse low-energy laser irradiation. Europhysics Letters. 2017 oct;119(3):35001. Available from: https://doi.org/10.1209/0295-5075/119/35001.

[41] Santos JJ, Vauzour B, Touati M, Gremillet L, Feugeas JL, Ceccotti T, et al. Isochoric heating and strong blast wave formation driven by fast electrons in solid-density targets. New Journal of Physics. 2017 oct;19(10):103005. Available from: https://doi.org/10.1088/1367-2630/aa806b.

[42] Batani KL, Malko S, Touati M, Feugeas JL, Lad AD, Jana K, et al. Characterization of blast waves induced by femtosecond laser irradiation in solid targets. High Power Laser Science and Engineering. 2024;12:e59. E59. Available from: https://www.cambridge.org/core/product/F1D2A97D6C40C4A4DB85084D784A2A44.

[43] Lucht J, Meyer P, Lohse LM, Salditt T. *HoToPy*: a toolbox for X-ray holo-tomography in Python. Journal of Synchrotron Radiation. 2025 Nov;32(6):1586-94. Available from: https://doi.org/10.1107/S1600577525008550.

[44] Yang L, Herbert ML, Baehtz C, Bouffetier V, Brambrink E, Dornheim T, et al. Scaling of thin wire cylindrical compression with material, diameter, and laser energy after 100 fs Joule surface heating. Matter and Radiation at Extremes. 2025 12;11(1):017604. Available from: https://doi.org/10.1063/5.0291405.

[45] Daun KJ, Thomson KA, Liu F, Smallwood GJ. Deconvolution of axisymmetric flame properties using Tikhonov regularization. Appl Opt. 2006 Jul;45(19):4638-46. Available from: https://opg.optica.org/ao/abstract.cfm?URI=ao-45-19-4638.

[46] Huang L, Šmíd M, Yang L, Humphries O, Hagemann J, Engler T, et al. Demonstration of full-scale spatiotemporal diagnostics of solid-density plasmas driven by an ultra-short relativistic laser pulse using an X-ray free-electron laser. Matter and Radiation at Extremes. 2025 10;11(1):017201. Available from: https://doi.org/10.1063/5.0279974.

[47] Huang L, Mishchenko M, Šmíd M, Humphries O, Preston TR, Pan X, et al.. Probing ultrafast heating and ionization dynamics in solid density plasmas with time-resolved resonant X-ray absorption and emission; 2025. Available from: https://arxiv.org/abs/2508.10627.

[48] Duchateau G, Pradel P, Bourdineaud N, Hébert D, Malaise F. Theoretical influence of ablator thickness on laser induced hydrodynamics in materials. Applied Physics A. 2025 Apr;131(5):355. Available from: https://doi.org/10.1007/s00339-025-08487-x.

[49] Abu-Shawareb H, Acree R, Adams P, Adams J, Addis B, Aden R, et al. Achievement of Target Gain Larger than Unity in an Inertial Fusion Experiment. Phys Rev Lett. 2024 Feb;132:065102. Available from: https://link.aps.org/doi/10.1103/PhysRevLett.132.065102.

[50] Hurricane OA. How ignition and target gain ¿1 were achieved in inertial fusion. High Energy Density Physics. 2024;53:101157. Available from: https://www.sciencedirect.com/science/article/pii/S157418182400082X.

[51] Hurricane OA, Allen A, Bachmann BL, Baker KL, Baxamusa S, Bhandarkar SD, et al. Present understanding of ignition and gain using indirect-drive inertial confinement fusion target designs on the U.S. National Ignition Facility. Plasma Physics and Controlled Fusion. 2024 dec;67(1):015019. Available from: https://doi.org/10.1088/1361-6587/ad994f.

[52] Casey DT, MacGowan BJ, Sater JD, Zylstra AB, Landen OL, Milovich J, et al. Evidence of Three-Dimensional Asymmetries Seeded by High-Density Carbon-Ablator Nonuniformity in Experiments at the National Ignition Facility. Phys Rev Lett. 2021 Jan;126:025002. Available from: https://link.aps.org/doi/10.1103/PhysRevLett.126.025002.

[53] Kraus D, Vorberger J, Pak A, Hartley N, Fletcher L, Frydrych S, et al. Formation of diamonds in laser-compressed hydrocarbons at planetary interior conditions. Nature Astronomy. 2017 Sep;1(9):606-11. Available from: https://doi.org/10.1038/s41550-017-0219-9.

[54] Frost M, McWilliams RS, Bykova E, Bykov M, Husband RJ, Andriambariarijaona LM, et al. Diamond precipitation dynamics from hydrocarbons at icy planet interior conditions. Nature Astronomy. 2024 Feb;8(2):174-81. Available from: https://doi.org/10.1038/s41550-023-02147-x.

[55] Kluge T, Rödel C, Rödel M, Pelka A, McBride EE, Fletcher LB, et al. Nanometer-scale characterization of laser-driven compression, shocks, and phase transitions, by x-ray scattering using free electron lasers. Physics of Plasmas. 2017 10;24(10):102709. Available from: https://doi.org/10.1063/1.5008289.

[56] Kluge T, Rödel M, Metzkes-Ng J, Pelka A, Garcia AL, Prencipe I, et al. Observation of Ultrafast Solid-Density Plasma Dynamics Using Femtosecond X-Ray Pulses from a Free-Electron Laser. Phys Rev X. 2018 Sep;8:031068. Available from: https://link.aps.org/doi/10.1103/PhysRevX.8.031068.

[57] Gaus L, Bischoff L, Bussmann M, Cunningham E, Curry CB, E J, et al. Probing ultrafast laser plasma processes inside solids with resonant small-angle x-ray scattering. Phys Rev Res. 2021 Dec;3:043194. Available from: https://link.aps.org/doi/10.1103/PhysRevResearch.3.043194.

[58] Ordyna P, Bähtz C, Brambrink E, Bussmann M, Laso Garcia A, Garten M, et al. Visualizing plasmons and ultrafast kinetic instabilities in laser-driven solids using X-ray scattering. Communications Physics. 2024 Sep;7(1):296. Available from: https://doi.org/10.1038/s42005-024-01776-6.

[59] Randolph L, Banjafar M, Preston TR, Yabuuchi T, Makita M, Dover NP, et al. Nanoscale subsurface dynamics of solids upon high-intensity femtosecond laser irradiation observed by grazing-incidence x-ray scattering. Phys Rev Res. 2022 Jul;4:033038. Available from: https://link.aps.org/doi/10.1103/PhysRevResearch.4.033038.

[60] Randolph L, Banjafar M, Yabuuchi T, Baehtz C, Bussmann M, Dover NP, et al. (Sub-)Picosecond Surface Correlations of Femtosecond Laser Excited Al-Coated Multilayers Observed by Grazing-Incidence X-ray Scattering. Nanomaterials. 2024;14(12). Available from: https://www.mdpi.com/2079-4991/14/12/1050.

[61] Randolph L, Özgül Öztürk, Ksenzov D, Huang L, Kluge T, Rahul SV, et al.. Probing laser-driven surface and subsurface dynamics via grazing-incidence XFEL scattering and diffraction; 2025. Available from: https://arxiv.org/abs/2509.12015.

[62] Glenzer SH, Redmer R. X-ray Thomson scattering in high energy density plasmas. Rev Mod Phys. 2009 Dec;81:1625-63. Available from: https://link.aps.org/doi/10.1103/RevModPhys.81.1625.

[63] Schörner M, Bethkenhagen M, Döppner T, Kraus D, Fletcher LB, Glenzer SH, et al. X-ray Thomson scattering spectra from density functional theory molecular dynamics simulations based on a modified Chihara formula. Phys Rev E. 2023 Jun;107:065207. Available from: https://link.aps.org/doi/10.1103/PhysRevE.107.065207.

[64] Gawne T, Moldabekov ZA, Humphries OS, Appel K, Baehtz C, Bouffetier V, et al. Ultrahigh resolution x-ray Thomson scattering measurements at the European X-ray Free Electron Laser. Phys Rev B. 2024 Jun;109:L241112. Available from: https://link.aps.org/doi/10.1103/PhysRevB.109.L241112.

[65] Dornheim T, Böhme M, Kraus D, Döppner T, Preston TR, Moldabekov ZA, et al. Accurate temperature diagnostics for matter under extreme conditions. Nature Communications. 2022 Dec;13(1):7911. Available from: https://doi.org/10.1038/s41467-022-35578-7.

[66] McBride EE, Krygier A, Ehnes A, Galtier E, Harmand M, Konôpková Z, et al. Phase transition lowering in dynamically compressed silicon. Nature Physics. 2019 Jan;15(1):89-94. Available from: https://doi.org/10.1038/s41567-018-0290-x.

[67] Pandolfi S, Brown SB, Stubley PG, Higginbotham A, Bolme CA, Lee HJ, et al. Atomistic deformation mechanism of silicon under laser-driven shock compression. Nature Communications. 2022 Sep;13(1):5535. Available from: https://doi.org/10.1038/s41467-022-33220-0.

[68] Pereira KA, Clarke SM, Singh S, Briggs R, McGuire CP, Lee HJ, et al. Stability of the fcc phase in shocked nickel up to 332 GPa. Nature Communications. 2025 May;16(1):4385. Available from: https://doi.org/10.1038/s41467-025-59385-y.

[69] Ohshima S, Nishimura H, Batani D, Desai T, Veltcheva M, Nakamura H, et al. Isochoric heating of low-Z, reduced-mass targets with high intensity laser pulse. Journal of Physics: Conference Series. 2010 aug;244(2):022054. Available from: https://doi.org/10.1088/1742-6596/244/2/022054.

[70] Kritcher AL, Swift DC, Döppner T, Bachmann B, Benedict LX, Collins GW, et al. A measurement of the equation of state of carbon envelopes of white dwarfs. Nature. 2020 Aug;584(7819):51-4. Available from: https://doi.org/10.1038/s41586-020-2535-y.

[71] Kraus D, Rips J, Schörner M, Stevenson MG, Vorberger J, Ranjan D, et al. The structure of liquid carbon elucidated by in situ X-ray diffraction. Nature. 2025 Jun;642(8067):351-5. Available from: https://doi.org/10.1038/s41586-025-09035-6.

[72] Zastrau U. Tackling Some Inertial Fusion Energy Challenges at the European XFEL. 2024;(REPORT. XFEL.EU WR-2024-001). Available from: http://xfel.tind.io/record/3916.

[73] Aglitskiy Y, Zulick C, Karasik M, Weaver JL, Velikovich AL, Schmitt AJ, et al. Absolute Hugoniot measurements in low-density plastic foams on the NIKE shock compression platform. Physics of Plasmas. 2025 10;32(10):102711. Available from: https://doi.org/10.1063/5.0294202.

[74] Millot M, Celliers PM, Sterne PA, Benedict LX, Correa AA, Hamel S, et al. Measuring the shock impedance mismatch between high-density carbon and deuterium at the National Ignition Facility. Phys Rev B. 2018 Apr;97:144108. Available from: https://link.aps.org/doi/10.1103/PhysRevB.97.144108.

[75] Millot M, Sterne PA, Eggert JH, Hamel S, Marshall MC, Celliers PM. High-precision shock equation of state measurements for metallic fluid carbon between 15 and 20 Mbar. Physics of Plasmas. 2020 10;27(10):102711. Available from: https://doi.org/10.1063/5.0007304.

[76] Cohen DH, MacFarlane JJ, Jaanimagi P, Landen OL, Haynes DA, Conners DS, et al. Tracer spectroscopy diagnostics of doped ablators in inertial confinement fusion experiments on OMEGA. Physics of Plasmas. 2004 05;11(5):2702-8. Available from: https://doi.org/10.1063/1.1647135.

[77] Kluge T, Hirsch-Passicos A, Schulz J, Frost M, Galtier E, Gauthier M, et al.. Microscopy X-ray Imaging enriched with Small Angle X-ray Scattering for few nanometer resolution reveals shock waves and compression in intense short pulse laser irradiation of solids; 2025. Available from: https://arxiv.org/abs/2511.10127.